

Photoinduced Melting of Antiferromagnetic Order in $\text{La}_{0.5}\text{Sr}_{1.5}\text{MnO}_4$ Measured Using Ultrafast Resonant Soft X-Ray Diffraction

H. Ehrke,^{1,2} R. I. Tobey,^{1,3} S. Wall,^{1,4} S. A. Cavill,² M. Först,³ V. Khanna,³ Th. Garl,³ N. Stojanovic,⁵ D. Prabhakaran,¹ A. T. Boothroyd,¹ M. Gensch,⁶ A. Mirone,⁷ P. Reutler,⁸ A. Revcolevschi,⁸ S. S. Dhesi,^{2,*} and A. Cavalleri^{1,3,†}

¹*Department of Physics, Clarendon Laboratory, University of Oxford, Oxford, United Kingdom*

²*Diamond Light Source, Chilton, Didcot, OX11 0QX, United Kingdom*

³*Max Planck Research Department for Structural Dynamics, University of Hamburg-CFEL, Hamburg, Germany*

⁴*Department of Physical Chemistry, Fritz Haber Institute, 14195 Berlin, Germany*

⁵*HASYLAB at DESY, Notkestrasse 85, 22607 Hamburg, Germany*

⁶*Helmholtz-Zentrum Dresden-Rossendorf, Bautzner Landstraße 400, 01328 Dresden, Germany*

⁷*European Synchrotron Radiation Facility, B.P. 220, F-38043 Grenoble, France*

⁸*Laboratoire de Physico-Chimie de l'Etat Solide, Centre Université Paris Sud, F-91405 Orsay Cedex, France*

(Received 11 January 2011; published 25 May 2011)

We used ultrafast resonant soft x-ray diffraction to probe the picosecond dynamics of spin and orbital order in $\text{La}_{0.5}\text{Sr}_{1.5}\text{MnO}_4$ after photoexcitation with a femtosecond pulse of 1.5 eV radiation. Complete melting of antiferromagnetic spin order is evidenced by the disappearance of a $(\frac{1}{4}, \frac{1}{4}, \frac{1}{2})$ diffraction peak. On the other hand, the $(\frac{1}{4}, \frac{1}{4}, 0)$ diffraction peak, reflecting orbital order, is only partially reduced. We interpret the results as evidence of destabilization in the short-range exchange pattern with no significant relaxation of the long-range Jahn-Teller distortions. Cluster calculations are used to analyze different possible magnetically ordered states in the long-lived metastable phase. Nonthermal coupling between light and magnetism emerges as a primary aspect of photoinduced phase transitions in manganites.

DOI: 10.1103/PhysRevLett.106.217401

PACS numbers: 78.70.Ck, 71.27.+a, 75.25.-j, 78.47.J-

Electronic order on nanometer length scales is a common feature of strongly correlated electron systems. Charges, spins, and orbitals form regular patterns to minimize the total potential energy while competing with the opposing tendency of electrons to become itinerant to minimize their kinetic energy [1]. Large-bandwidth manganites, like $\text{La}_{1-x}\text{Sr}_x\text{MnO}_3$, are a typical example of such competition, with the antiferromagnetic (AF) Mott insulating parent compound (LaMnO_3) transforming into a double-exchange metallic ferromagnet for hole doping between $0.2 \leq x \leq 0.5$ and again into complex insulating phases with charge and orbital ordering for commensurate doping levels (e.g., $x = \frac{1}{2}$). Since the energy difference between these phases is very small, doped manganites can be controlled reversibly with external stimuli such as magnetic fields [2–4], pressure [5], electric currents [6], and light [7–12]. In particular, photoexcitation transfers charge across semicovalent bonds, drastically perturbing spin and orbital order [13], enabling optical control of magnetism in manganites and related materials.

Despite the great interest in photoinduced phenomena, a comprehensive understanding of the underlying physics is missing. This is particularly elusive because charge, spin, and orbital arrangements are interdependent degrees of freedom, evolving on ultrafast time scales and nanometer length scales, and are thus difficult to disentangle as they evolve in time. Transient electronic orders can therefore be probed only with ultrafast techniques sensitive to nanometer-scale modulations of charge and spin

densities. These modulations are typically small perturbations of the total charge at each atomic site and are not accessible with any time-resolved optical or x-ray probe used to date [14–16]. Recently, static electronic order in manganites has been probed with resonant soft x-ray diffraction (RSXD), which is directly sensitive to electronic states close to the Fermi level using photon energies resonant with the $2p \rightarrow 3d$ dipole transitions (Mn $L_{2,3}$ edges). Furthermore, the energy dependence of the RSXD intensity can be used to understand the competing interactions leading to spin and orbital ordering [17–22].

In this Letter, we have extended RSXD to the ultrafast time scale and separated ultrafast spin and orbital dynamics in the single-layer, half-doped manganite $\text{La}_{0.5}\text{Sr}_{1.5}\text{MnO}_4$. This is achieved by detecting changes in the time-dependent diffraction intensity at two different scattering peaks which reflect spin and orbital order periodicities independently. Our results demonstrate that light excitation completely removes spin order in a nonthermal manner while only weakly perturbing orbital order.

Samples of $\text{La}_{0.5}\text{Sr}_{1.5}\text{MnO}_4$ were grown by using the floating zone technique from a stoichiometric powder. Crystals were oriented along the [110] ([112]) direction for the orbital (spin) order measurements and polished with diamond paste to an optical finish. The magnetic properties of the samples were verified by using SQUID magnetometry. The sample temperature was held at 25 K, i.e., below the charge or orbital ordering temperature ($T_{\text{CO-OO}} = 220$ K) and Néel temperature ($T_N = 110$ K).

In this CE-type antiferromagnetic phase, charge, spins, and orbitals form a characteristic pattern, well visualized as a set of antiferromagnetically coupled ferromagnetic (FM) zigzag chains of $3x^2 - r^2$ ($3y^2 - r^2$) orbitals at the Mn^{3+} sites [23,24]. Trains of 100 fs, 800 nm wavelength ($h\nu = 1.5$ eV) optical pulses at a repetition rate of 20 kHz were synchronized to soft x-ray pulses at beam line I06, Diamond Light Source. Optical-pump-RSXD-probe experiments measured time-dependent $(\frac{1}{4}, \frac{1}{4}, \frac{1}{2})$ and $(\frac{1}{4}, \frac{1}{4}, 0)$ diffraction peaks which reflect the time-dependent spin and orbital ordering, respectively [17,18,25]. These soft x-ray diffraction peaks were resolved by using photon counting electronics by gating only those pulses synchronous with the laser pulses, i.e., <1 probe pulse out of every 20 000. The laser pump beam was focused to a FWHM spot size of ~ 170 μm , whereas the x-ray beam was focused to a spot size of ~ 100 μm to ensure that the pumped volume was greater than the probed volume (the laser penetration depth was calculated to be a factor of ~ 2 more than the x-ray penetration depth by using absorption spectroscopy results [26,27]). The static RSXD energy dependencies, as well as those measured at negative pump-probe time delays, were in good agreement with the literature [17,18,22,25].

Figures 1(a) and 1(b) show the photon-energy dependence of the $(\frac{1}{4}, \frac{1}{4}, \frac{1}{2})$ and $(\frac{1}{4}, \frac{1}{4}, 0)$ diffraction peak intensity before and 200 ps after the laser pump pulse. For all excitation fluences above 5 mJ/cm^2 , the $(\frac{1}{4}, \frac{1}{4}, \frac{1}{2})$ peak entirely vanished, leaving only a weak signal due to fluorescence. In contrast, the photoinduced reduction of the $(\frac{1}{4}, \frac{1}{4}, 0)$ peak is less than 25% at the saturation fluence of the $(\frac{1}{4}, \frac{1}{4}, \frac{1}{2})$ peak (5 mJ/cm^2). Figure 2(a) shows the time-dependent changes in the scattered intensity ($\Delta I/I_s$) as a function of time delay after excitation. Intensity changes

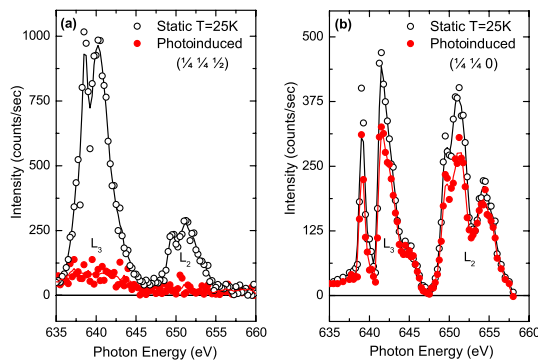


FIG. 1 (color online). (a) Energy dependence of the $(\frac{1}{4}, \frac{1}{4}, \frac{1}{2})$ diffraction peak intensity before (open circles) and 200 ps after photoexcitation (closed red circles) using a laser fluence of 5.5 mJ/cm^2 . The lines represent smoothed fits to the data. (b) Energy dependence of the $(\frac{1}{4}, \frac{1}{4}, 0)$ diffraction peak intensity before (open circles) and 200 ps after photoexcitation (closed red circles) using a laser fluence of 10 mJ/cm^2 . The lines represent smoothed fits to the data.

were recorded at $h\nu = 640.25$ eV for the $(\frac{1}{4}, \frac{1}{4}, \frac{1}{2})$ magnetic reflection and at $h\nu = 641.5$ eV for the $(\frac{1}{4}, \frac{1}{4}, 0)$ orbital reflection, i.e., at the maximum scattering intensities for the respective diffraction peaks. The scattered intensities were reduced within the time resolution of the x-ray probe (~ 50 ps) and did not recover within the time window available by using a mechanical delay stage (~ 500 ps).

The temporal resolution of our experiments was improved by operating the storage ring in low- α mode, in which shorter x-ray pulses (~ 9 ps) were generated by compressing the electron bunches in the ring at the expense of total current and x-ray flux. Already on the sub-10 ps time scale the magnetic $(\frac{1}{4}, \frac{1}{4}, \frac{1}{2})$ diffraction peak promptly disappears [Figs. 3(a) and 3(b)]. Longer time scales, up to 1 μs , were probed by electronically controlling the pump-probe separation out to microsecond delays. Figures 3(c) shows that the $(\frac{1}{4}, \frac{1}{4}, \frac{1}{2})$ diffraction peak intensity returns back towards the static value with at least three time scales. The red line in Fig. 3(c) shows a fit using two exponentials with time constants of 10 and 110 ns. A much longer time scale is also visible as a plateau at about 15% of the diffraction peak intensity loss.

We first note that spin and orbital order rearrange differently upon static heating and that, if the temperature were to exceed T_N , the $(\frac{1}{4}, \frac{1}{4}, \frac{1}{2})$ reflection would vanish while the $(\frac{1}{4}, \frac{1}{4}, 0)$ reflection would only gradually decrease in intensity up to $T_{\text{CO/OO}}$ [22]. However, this does not explain our observations. First, a conservative estimate of the temperature increase shows that the changes in sample temperature remain well below T_N and hence nonthermal [27]. Not only

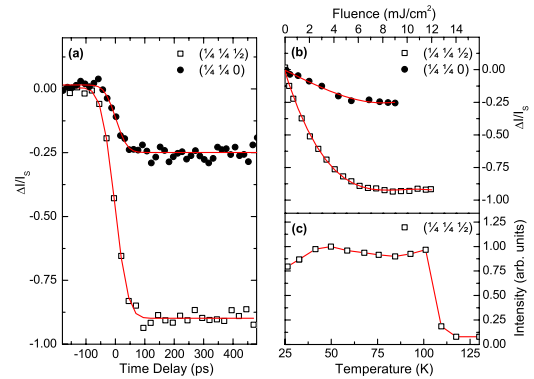


FIG. 2 (color online). (a) Time dependence of the $(\frac{1}{4}, \frac{1}{4}, \frac{1}{2})$ diffraction peak intensity recorded at $h\nu = 640.25$ eV with a laser fluence of 5.5 mJ/cm^2 (open squares) and the $(\frac{1}{4}, \frac{1}{4}, 0)$ diffraction peak intensity recorded at $h\nu = 641.5$ eV (closed circles) with a laser fluence of 10 mJ/cm^2 . (b) Fluence dependence of the $(\frac{1}{4}, \frac{1}{4}, \frac{1}{2})$ (open squares) and $(\frac{1}{4}, \frac{1}{4}, 0)$ (closed circles) diffraction peak intensity 200 ps after photoexcitation. (c) Temperature dependence of the $(\frac{1}{4}, \frac{1}{4}, \frac{1}{2})$ diffraction peak intensity measured statically. Fluence and temperature dependences are aligned by calculating the sample temperature increase for each irradiation fluence. The red lines are guides to the eye.

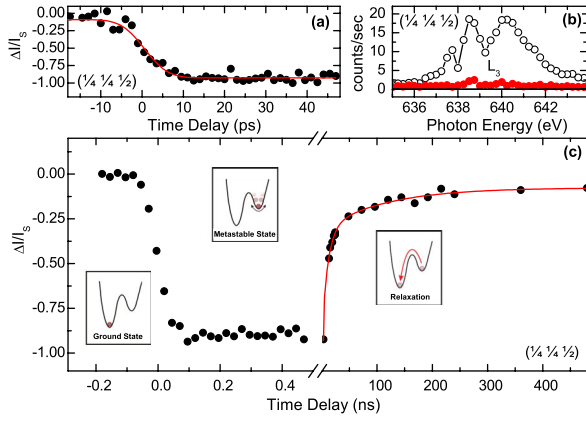


FIG. 3 (color online). (a) Time dependence of the $(\frac{1}{4}, \frac{1}{4}, \frac{1}{2})$ diffraction peak intensity measured at $h\nu = 640.25$ eV in low- α mode. The red line shows a fit to the data using an error function with a FWHM of 10 ps. (b) Energy dependence of the $(\frac{1}{4}, \frac{1}{4}, \frac{1}{2})$ diffraction peak intensity before (open circles with line) and 20 ps after photoexcitation (closed red circles with line). (c) Decay of the photoinduced state (closed circles), together with a double exponential fit (red line). The schematic diagrams for the free energy landscape depict the existence of a CE ground state (left side) and of a metastable state (spin-disordered or ferromagnetic) protected by a kinetic barrier.

is the maximum possible temperature increase well below T_N , but the dependence of the diffraction peak intensities on the laser fluence [see Fig. 2(b)] scales very differently to that expected for heating. In Fig. 2(c), the temperature dependence of the $(\frac{1}{4}, \frac{1}{4}, \frac{1}{2})$ diffraction peak intensity is reported for comparison, with the horizontal scales aligned to the fluence dependence shown in Fig. 2(b) by calculating the sample heating for each fluence. Particularly striking is the weak excitation regime in which we measure a significant photoinduced drop in diffraction peak intensity already for 0.66 mJ/cm², whereas the thermal response of the magnetic peak is temperature-independent at this point.

Thus, the rearrangement must be strongly influenced by the nonthermal physics occurring immediately after optical excitation. Because of the strong on-site Hund's rule coupling, excitation with linearly polarized light at 1.5 eV can result only in transitions between ferromagnetically coupled sites, transferring e_g electrons between Mn^{3+} and Mn^{4+} sites along the ferromagnetic chains [28]. Figure 4(a) reports a caricature of such an excitation, which transforms $\text{Mn}^{4+}/(\text{Mn}^{3+}/\text{Mn}^{4+})/\text{Mn}^{3+}$ chains into $\text{Mn}^{4+}/(\text{Mn}^{4+}/\text{Mn}^{3+})/\text{Mn}^{3+}$ chains, effectively creating charge defects. This excitation triggers distortions of the lattice by rearranging the Jahn-Teller energy at each site. Furthermore, significant modification of the exchange pattern is expected [13]. According to the Goodenough-Kanamori-Anderson rules, the exchange pattern along the chains, which is FM/FM/FM in the $\text{Mn}^{4+}/(\text{Mn}^{3+}/\text{Mn}^{4+})/\text{Mn}^{3+}$ ground state, is expected to switch to AF/FM/AF in the $\text{Mn}^{4+}/(\text{Mn}^{4+}/\text{Mn}^{3+})/\text{Mn}^{3+}$

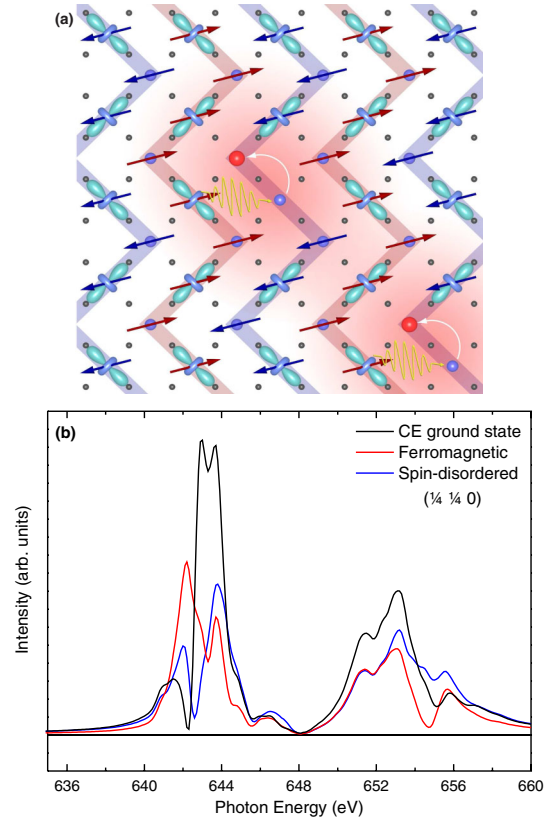


FIG. 4 (color online). (a) Schematic of charge, spin, and orbital order in $\text{La}_{0.5}\text{Sr}_{1.5}\text{MnO}_4$ indicating the ferromagnetic zigzag chains which are antiferromagnetically coupled to each other. After laser photoexcitation, using 1.5 eV light, defects are created due to the transfer of e_g electrons from the Mn^{3+} sites to the Mn^{4+} sites along the ferromagnetic zigzag chains. (b) Calculated energy dependence of the $(\frac{1}{4}, \frac{1}{4}, 0)$ diffraction peak intensity for the ground state (black line) and for two types of metastable states: ferromagnetic alignment (red line) and a spin-disordered state (blue line).

excited state. It is then possible that the long-lived product phase relaxes into a metastable spin-disordered or even ferromagnetic phase or a mixture of the two. We note that the possibility of a photoinduced ferromagnetic state has also been raised recently by using ultrafast magneto-optical Kerr measurements in related compounds [29].

In order to more fully understand the product phase, we performed cluster calculations with the 3d states of a central active Mn^{3+} site coupled to the neighboring oxygen p orbitals by a hopping term modulated by Slater-Koster parameters [20]. The in-plane oxygen p orbitals were coupled to the 3d states of the neighboring Mn^{4+} sites. We first considered the case of a spin-disordered excited state. This consisted of a superposition between different $|\mathbf{S}| = 2$ states, i.e., maintaining the same high-spin configuration of the ground state, but with S_z taking all five possible values $S_z = -2, -1, 0, 1, 2$ at different sites. A second possible state was also considered in which the spin alignment was ferromagnetic on all sites. In both

cases, we left the Jahn-Teller distortion unperturbed, considering that excitations would leave the average charge occupancy unperturbed and would primarily affect short-range correlations. Both spin-disordered and ferromagnetic states were found to have an average excess energy of a few tens of meV and are accessible after the photoexcited system has thermalized [29].

To directly compare the cluster simulations to our experimental results, we calculated the resonant scattering intensities from these transient magnetic states by using the same procedure discussed in Ref. [20]. Figure 4(b) shows the calculated energy dependence for the $(\frac{1}{4}, \frac{1}{4}, 0)$ diffraction peak for the ground state, as well as for the spin-disordered and ferromagnetic states. The calculated $(\frac{1}{4}, \frac{1}{4}, 0)$ orbital diffraction intensity remained high at all energies, due to the Jahn-Teller distortion in the calculation for the excited state. Evidence for a residual Jahn-Teller orbital ordering also comes from the energy dependence of the experimental $(\frac{1}{4}, \frac{1}{4}, 0)$ diffraction peak intensity of Fig. 1(b), which is reduced more at the two lower energy Mn L_3 and L_2 edge peaks [22]. Importantly, we find that both states (spin-disordered and ferromagnetic) give rise to similar integrated scattering intensities for the $(\frac{1}{4}, \frac{1}{4}, 0)$ peak and that, based on the available data, we cannot determine if the long-lived photoexcited state is spin-disordered or ferromagnetic. Time-resolved x-ray magnetic circular dichroism [30,31] might provide us with an answer by detecting any net magnetization that develops. The long lifetimes needed for relaxation are consistent with either of these magnetic states. The reformation of the CE phase, too slow to be caused by thermal diffusion [32], occurs across a kinetic barrier and requires nucleation and domain propagation to be complete. This is schematically depicted in a caricature of the free energy landscape in Fig. 3(c). The system starts in the CE antiferromagnetic ground state and is driven nonthermally into a metastable phase before relaxing back to the ground state at longer time scales.

In summary, we have used time-resolved RSXD to probe the microscopic spin and orbital order in photoexcited $\text{La}_{0.5}\text{Sr}_{1.5}\text{MnO}_4$. Photoexcitation perturbs spin ordering, while the Jahn-Teller distortions and resulting orbital order remain largely unaffected. Time-resolved RSXD has therefore proven to be especially effective in separating spin dynamics from Jahn-Teller contributions. In the future, measurements using free electron lasers will allow access to coherences at extreme time scales, including lattice [13], orbital [11], and charge [33] degrees of freedoms.

We thank R. A. Mott for expert technical assistance.

*dhesi@diamond.ac.uk

†andrea.cavalleri@mpsd.cfel.de

[1] J. B. Goodenough, *Phys. Rev.* **100**, 564 (1955).

- [2] R. M. Kusters *et al.*, *Physica (Amsterdam)* **155B**, 362 (1989).
- [3] R. von Helmolt *et al.*, *Phys. Rev. Lett.* **71**, 2331 (1993).
- [4] A. Asamitsu *et al.*, *Nature (London)* **373**, 407 (1995).
- [5] H. Y. Hwang *et al.*, *Phys. Rev. Lett.* **75**, 914 (1995).
- [6] A. Asamitsu *et al.*, *Nature (London)* **388**, 50 (1997).
- [7] V. Kiriukhin *et al.*, *Nature (London)* **386**, 813 (1997).
- [8] K. Myano *et al.*, *Phys. Rev. Lett.* **78**, 4257 (1997).
- [9] M. Rini *et al.*, *Nature (London)* **449**, 72 (2007).
- [10] R. I. Tobey *et al.*, *Phys. Rev. Lett.* **101**, 197404 (2008).
- [11] D. Polli *et al.*, *Nature Mater.* **6**, 643 (2007).
- [12] M. Fiebig *et al.*, *Science* **280**, 1925 (1998).
- [13] S. Wall *et al.*, *Phys. Rev. Lett.* **103**, 097402 (2009).
- [14] T. Ogasawara *et al.*, *Phys. Rev. B* **63**, 113105 (2001).
- [15] P. Beaud *et al.*, *Phys. Rev. Lett.* **103**, 155702 (2009).
- [16] M. Rini *et al.*, *Phys. Rev. B* **80**, 155113 (2009).
- [17] S. S. Dhesi *et al.*, *Phys. Rev. Lett.* **92**, 056403 (2004).
- [18] S. B. Wilkins *et al.*, *Phys. Rev. Lett.* **91**, 167205 (2003).
- [19] C. W. M. Castleton and M. Altarelli, *Phys. Rev. B* **62**, 1033 (2000).
- [20] A. Mirone *et al.*, *Eur. Phys. J. B* **53**, 23 (2006).
- [21] M. Garcia-Fernandez *et al.*, *Phys. Rev. B* **77**, 060402 (2008).
- [22] U. Staub *et al.*, *Europhys. Lett.* **76**, 926 (2006).
- [23] B. J. Sternlieb *et al.*, *Phys. Rev. Lett.* **76**, 2169 (1996).
- [24] A. Daoud-Aladine *et al.*, *Phys. Rev. Lett.* **89**, 097205 (2002).
- [25] U. Staub *et al.*, *Phys. Rev. B* **71**, 214421 (2005).
- [26] R. Nakajima, J. Stöhr, and Y. U. Idzerda, *Phys. Rev. B* **59**, 6421 (1999).
- [27] We calculate an upper limit for laser-induced heating, reached at equilibrium between the electrons and lattice. From optical-conductivity data we extract the temperature-dependent optical absorption depth at 800 nm and calculate that a maximum energy density of 72 J/cm³ thermalizes in the 65 nm absorption depth for each mJ/cm² of incident laser fluence. In the absence of heat diffusion, this corresponds to a ~14 K temperature increase for 1 mJ/cm² at 25 K base temperature, where the heat capacity is about 5 J/(K cm³). As the base temperature increases, higher heat capacities [reaching 19 J/(K cm³) at 100 K] lead to lower heating. The combined temperature increase for 5 mJ/cm² excitation fluence is ~60 K. We stress that this is overestimated, since carrier and heat diffusion will transport some of the energy into the bulk before thermalization.
- [28] Y. Okimoto *et al.*, *Phys. Rev. B* **59**, 7401 (1999).
- [29] Higher-lying states were also explored, although no notable state was found up to a 0.7 eV crystal-field excitation where the e_g electron rotates to the c axis. At still higher excess energies, states with a spin-flipped t_{2g} electron replace the e_g electron at the active Mn³⁺ ion. While these states may be important at the earliest times, we have excluded them from the contributors to the metastable state.
- [30] C. Stamm *et al.*, *Nature Mater.* **6**, 740 (2007).
- [31] C. Boeglin *et al.*, *Nature (London)* **465**, 458 (2010).
- [32] A. Oleaga *et al.*, *Phys. Rev. B* **70**, 184402 (2004).
- [33] S. Wall *et al.*, *Nature Phys.* **7**, 114 (2011).